ACS APPLIED MATERIALS & INTERFACES

Research Article

www.acsami.org

Toxicity of Nano Molybdenum Trioxide toward Invasive Breast Cancer Cells

Thao Anh Tran,[‡,†] Karthikeyan Krishnamoorthy,[‡,§] Yeon Woo Song,[†] Somi Kim Cho,*[,†] and Sang Jae Kim*[,§,∥]

[†]Faculty of Biotechnology, College of Applied Life Sciences, Jeju National University, Jeju, Jeju − 690 756, Republic of Korea

[§]Nanomaterials and System Laboratory, Department of Mechanical Engineering, Jeju National University, Jeju, Jeju − 690 756, Republic of Korea

[∥]Nanomaterials and System Laboratory, Department of Mechatronics Engineering, Jeju National University, Jeju, Jeju − 690 756, Republic of Korea

Supporting Information

ABSTRACT: Current chemotherapy is limited by the nature of invasive cancer cells, which are similar to cancer stem cells. Nanomaterials provide a potential alternate mode of cancer therapy. This study investigated the cytotoxicity of molybdenum trioxide (MoO_3) nanoplates toward invasive breast cancer iMCF-7 cells by analyzing morphological changes and performing Western blot and flow cytometry analyses. The findings suggested that MoO_3 exposure induces apoptosis and generates reactive oxygen species (ROS) in iMCF-7 cells. This study revealed the potential utility of MoO_3 for treating metastatic cancer cells, which might enable advancements in cancer therapy.

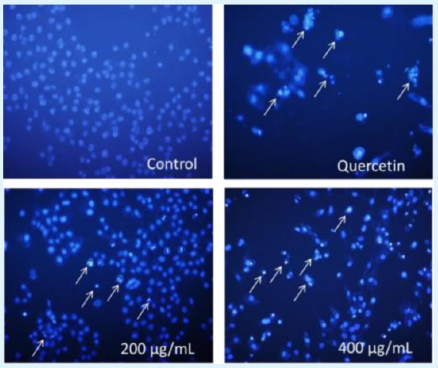

KEYWORDS: *molybdenum trioxide, cancer therapy, invasive cells, apoptosis, reactive oxygen species*

1. INTRODUCTION

Cancer is a major disease worldwide, killing about more than 1500 people daily in the United States according to the American Cancer Society (ACS, 2012).[1] Cancer mortality results from cell motility and the self-renewal of invasive and stem-cancer cells, which lead to chemotherapy failure.[2] Researchers are developing novel alternatives for cancer chemotherapy. Nanomaterials have shown potential for the treatment of cancer due to their ability to overcome cell motility and stemness characteristics.[3,4] The use of nanostructured materials as an alternative to conventional chemotherapy is an area of emerging interest due to their selective toxicity.[5] The toxicity of nanoparticles (NPs) toward cancer cells depends on several factors, such as the size, shape, and surface chemistry of the NPs, the specific cellular systems, and the interactions among them.[6] Nanoassisted cancer therapy includes 1) the controlled delivery of drugs/photosensitizers to reduce the side effects of chemo/photodynamic therapy,[7] 2) targeted drug delivery to kill specific cancer cells,[8] 3) magnetic hyperthermia,[9] 4) nano cryosurgery,[10] 5) sonodynamic therapy,[11] 6) photothermal therapy,[12] and 7) sonophotodynamic therapy.[13] Fundamental research involves the development of novel materials and the study of their toxicity toward cancer cells and the mode of cell death. This will lead to the development of materials for basic research in the biological sciences and clinical medicine.

The use of metal and metal oxide nanomaterials in cancer therapy has been studied recently. The cytotoxic effects of silver and gold NPs on various cancer cell types have been explored.[14,15] Similarly, metal oxides such as ZnO, TiO_2, CeO_2, and CuO show selective toxicity toward cancer cells.[4,16−18] Previously, we demonstrated that MgO led to the apoptosis of cancer cells via elevated reactive oxygen species (ROS) levels.[19] The increasing death rates due to cancer and failure and side effects of chemotherapeutic drugs motivate researchers to develop new nanomaterials for cancer therapy. In this regard, interest has focused on molybdenum trioxide (MoO_3) nanostructures because of their multifunctional properties in photocatalysis, as an electrochemical capacitor and an oxidative catalyst, and antibacterial applications.[20,21] Molybdenum is an essential trace element in humans and mammals and acts as a cofactor for various enzymes, such as aldehyde oxidase, xanthine oxidase, and sulfite oxidase.[22] Dietary molybdenum deficiency leads to increased rates of esophageal cancer.[23] Molybdenum(VI) complexes are effective antidiabetic agents.[24] Our recent study demonstrated the antibacterial activity of MoO_3 toward pathogenic bacteria.[25] Some previous studies have demonstrated that MoO_3 is less

Received: December 5, 2013
Accepted: January 13, 2014
Published: January 13, 2014

cytotoxic than silver NPs. Hussain et al. demonstrated that MoO_3 NPs are less toxic than silver NPs against BRL 3A rat liver cells.[26] Stolle et al. showed that MoO_3 is less toxic than Ag NPs against a mouse spermatogonial stem cell line.[27] Recent studies of polyoxomolybdates (a structure containing discrete molybdenum oxide anion clusters) showed their potential antitumor activity toward pancreatic and gastric cancer cells.[28,29] Although many applications of MoO_3 NPs in various forms have been studied in biological systems in the past decade, no studies have examined the cytotoxic effects of nano MoO_3 toward cancer cells. Hence, a detailed study of the toxicity of MoO_3 nanomaterials in cancer cells would be of immense interest. Therefore, this study explored the cytotoxicity of MoO_3 nanoplates toward invasive breast cancer iMCF-7 cells and investigated the mechanism of cell death.

2. EXPERIMENTAL SECTION

2.1. Materials Used. Ammonium molybdate tetrahydrate and hydrochloric acid were purchased from Daejung Chemicals, South Korea. All chemicals were of research grade and used without further purification.

2.2. Preparation of MoO_3 Nanoplates. The MoO_3 nanoplates were prepared by a wet chemical method using ammonium molybdate as the starting precursor. Briefly, 3.6 g of ammonium molybdate were dissolved in water and acidified using HCl until the solution reached a pH of 1. Then, the solution was stirred vigorously using a Teflon-coated magnetic bar at about 80 °C for 2 h, which resulted in the precipitation of molybdic acid. The precipitate was washed thoroughly with distilled water and centrifuged at 5000 rpm for 10 min to remove residuals. The washing was repeated several times until the precipitate was free from trace impurities. The purified precipitate was dried in a hot-air oven at 100 °C to remove water and calcined at 500 °C, which resulted in the formation of MoO_3 nanoplates.

2.3. Characterization of MoO_3 Nanoplates. The phase purity and crystalline size of the MoO_3 nanoplates were determined using a Rigaku X-ray diffractometer (XRD) operated at 40 keV and 40 mA with Cu−Kα radiation in the range of 10−50°. A Cary Eclipse fluorescence spectrophotometer was used to examine the photoluminescence (PL) of the synthesized MoO_3. The morphology of the synthesized MoO_3 nanoplates was evaluated by field-emission scanning electron microscopy (FE-SEM; JSM-6700F, JEOL) and high-resolution transmission electron microscopy (HR-TEM; FEI Titan 80-300 under a maximum acceleration voltage of 200 kV).

2.4. Reagents. RPMI 1640 medium, Dulbecco's modified Eagle's medium (DMEM), F12 medium, bovine serum albumin (BSA), trypsin/EDTA, fetal bovine serum (FBS), and 100× antibiotic-antimycotic were purchased from Invitrogen. Hoechst 33342, dimethyl sulfoxide (DMSO), 3-(4,5-dimethylthiazol-2-yl)-2,5-diphenyltetrazolium bromide (MTT), propidium iodide (PI), and RNase A were purchased from Sigma Chemical (St. Louis, MO). The Annexin V-FITC Apoptosis Detection Kit I and BD™ MitoScreen (JC-1) Kit were purchased from BD Biosciences (Franklin Lakes, NJ). Anticaspase 8, -caspase 9, -Bax, -Bcl-2, and -actin antibodies were purchased from Cell Signaling (Danvers, MA). Polyvinylidene fluoride (PVDF) membranes for Western blotting were purchased from Bio-Rad (Hercules, CA). All chemicals were dissolved in DMSO, except MoO_3, which was dissolved in phosphate-buffered saline (PBS).

2.5. Cell Lines and Cell Culture. Human invasive breast cancer cells iMCF-7 were isolated with $CD44^{high}/CD24^{low}$ marker from normal breast cancer MCF-7, enriched, and characterized in Stem cell laboratory of Vietnam-HCM National University (details given in SI Figure S1−S3). iMCF-7 and keratinocyte HaCaT cells were cultured in RPMI-1640; normal breast cancer MCF-7 cells were cultured in DMEM mix F12 media, supplemented with 10% fetal bovine serum (FBS) and 1% antibiotics at 37 °C in a humidified atmosphere containing 5% CO_2.

2.6. Cell Viability Assay. The effect of MoO_3 nanoplates on cell viability was determined using the MTT assay.[30,31] Briefly, cells (3×10^4 cells/mL) were seeded in 96-well plates in 200 μL of medium containing antibiotics and 10% FBS. After 24 h, the cells were treated with different concentrations of MoO_3. After 48 h, we added 20 μL of MTT solution (5 mg/mL) to each well followed by incubation in a humidified environment for 4 h. Then, the supernatant was removed and 150 μL of DMSO was added. The plates were shaken in the dark for 30 min and then measured using a Sunrise microplate reader (Tecan; Salzburg, Austria) at an absorbance wavelength of 570 nm. Cell viability is shown as the percentage of the control viability (mean ± SD). The blank contained 200 μL of RPMI 1640 or DMEM-F12 with 10% FBS and equivalent reagent concentrations. All experiments were conducted in triplicate.

2.7. Analysis of Morphological Changes. The apoptotic behavior and morphological changes of iMCF-7 cells after exposure to MoO_3 nanoplates were studied using Hoechst 33342 staining.[18,32] Briefly, cells were seeded in 6-well plates and treated with MoO_3 for 48 h. Then, the treated cells were stained with 10 μM Hoechst and observed under a fluorescence microscope (Olympus, Essex, UK).

2.8. Cytometric Analysis. To analyze the cell cycle distribution, apoptosis, and mitochondrial membrane potential, cells (3×10^4 cells/mL) were plated in 60-mm dishes and treated with MoO_3 for 48 h. An Annexin V-FITC Apoptosis Detection Kit I was used to detect apoptosis and necrosis by detecting phosphatidylserine translocation from the inner to the outer plasma membrane. The apoptosis was detected with annexin V, whereas necrotic cells are permeable to PI.[19] The cells were washed with PBS, detached using Trypsin-EDTA, harvested, diluted in buffer containing annexin V and PI, and incubated for 15−20 min at room temperature (RT). For JC-1 mitochondrial membrane detection, the treated cells were harvested and stained with JC-1 for 10−15 min in an incubator and washed twice with 1× assay buffer at RT. For cell cycle analysis, the treated cells were harvested, washed with PBS, fixed with 70% cold ethanol overnight, rehydrated in 2 mM EDTA-PBS, treated with RNase A (25 ng/mL), and stained with PI (10 mg/mL). For ROS detection, the cells were treated with MoO_3 (200 or 400 μg/mL) for 48 h and then incubated with 2′,7′-dichlorodihydrofluorescein diacetate (H2DCFDA) for 30 min at 37 °C. Then, the cells were harvested and washed with PBS.[19] All analyses were performed using a FACSCaliber flow cytometer (BD Biosciences). For each sample, 10,000 cells were counted and the data analyzed using CellQuest software (BD Biosciences).

2.9. Western Blot Analysis. After 48 h, the cells were collected, lysed in lysis buffer (100 mM Tris-HCl [pH 8], 250 mM NaCl, 0.5% NP-40, and 1× protease inhibitor cocktail), sonicated a few times, and then kept on ice for 30 min. The cell lysates were centrifuged at 13,000 rpm for 30 min at 4 °C. The supernatant was collected, and the concentration was determined using a BCA™ Protein assay (Pierce; Rockford, IL). Aliquots of the lysate were separated by 10−15% sodium dodecyl sulfate-polyacrylamide gel electrophoresis (SDS-PAGE) and transferred to PVDF membranes using glycine transfer buffer (192 mM glycine, 25 mM Tris-HCl [pH 8.8] and 20% [v/v] methanol). After blocking with 5% skim milk overnight at 4 °C or at RT for 1 h, the membrane was incubated with primary antibodies for 1 h at RT or overnight at 4 °C and then for 1 h with secondary antibodies. The primary antibodies were diluted 1:1000, whereas the anti-β-actin primary and secondary antibodies (horseradish peroxidase-conjugated goat antimouse IgG) (Vector Laboratories; Burlingame, CA) were diluted 1:10,000. Protein bands were detected using the WEST-ZOL plus Western Blot Detection System (iNtRON, Gyeonggi-do, Korea).[33]

2.10. Statistical Analysis. All data presented are the result of at least three replicates. Values are expressed as the mean ± SD.

3. RESULTS AND DISCUSSION

This study used a precipitation method to prepare MoO_3 nanoplates using ammonium molybdate as the starting precursor and concentrated HCl. Figure 1 shows the XRD pattern of the synthesized MoO_3 nanoplates. The diffraction pattern and interplanar spacing of the MoO_3 nanoplates closely

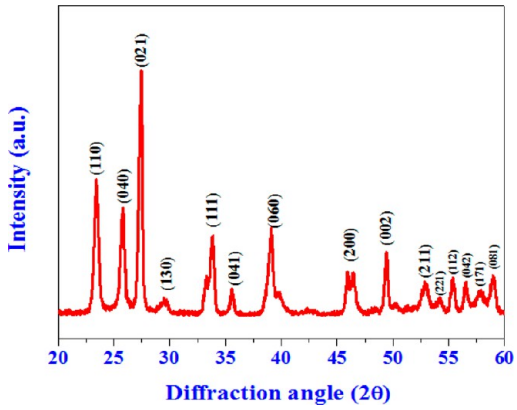

Figure 1. X-ray diffraction pattern of MoO_3 nanoplates.

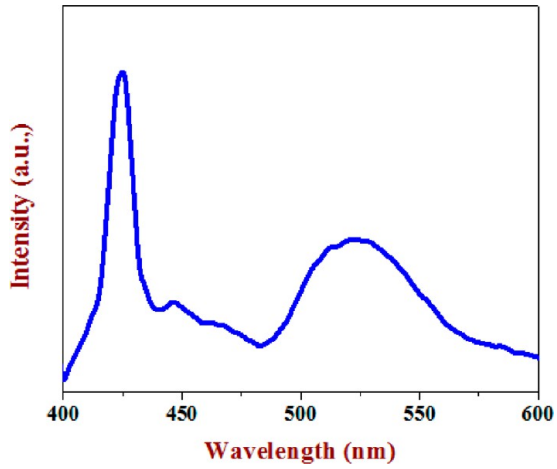

Figure 3. Photoluminescence spectrum of MoO_3 nanoplates.

matched the orthorhombic structure of MoO_3 (International Centre for Diffraction Data, JCPDS file no. 05-0508).[34] The very strong intensity of the (021) plane in the XRD pattern of MoO_3 indicates the crystal orientation along the [001] direction. In addition, no characteristic peaks of impurities were detected in the XRD pattern, suggesting that the MoO_3 nanoplates synthesized using this method were of high quality. Figure 2(a) is an FE-SEM micrograph showing the presence of plate-like MoO_3 nanostructures. Figure 2(b) shows the HR-TEM image of the MoO_3 nanoplates. The nanoplates were 400 nm long and 100−200 nm wide. The nanoplate-like structures form via the thermal decomposition of molybdic acid into MoO_3.[35] Clear diffraction spots observed in the selected-area election diffraction (SAED) pattern (Figure 2(c)) can be indexed to the [010] zone of MoO_3, indicating preferential growth along the *c*-axis.[35]

Defects and oxygen vacancies act as invisible agents that can significantly alter the electronic, optical, and biological properties of nanomaterials.[36] Therefore, the presence of defects or oxygen vacancies on the MoO_3 surface is very significant. Hence, we studied the PL of MoO_3 (Figure 3). The spectra revealed a sharp peak around 424 nm and a broad band around 530 nm. The emission at 424 nm is due to the band−band transition of the semiconductor and concurs with a previous report.[37] The broad band around 530 nm is due to deep-level emissions caused by the presence of Mo interstitials, surface defects, and oxygen vacancies. This agrees with Navas et al., illustrating visible light emission in MoO_3 thin films due to deep-level excitation.[38] The presence of oxygen vacancies in the MoO_3 surface might be due to incomplete oxidation or adsorbed oxygen. These studies indicate the presence of oxygen vacancies in the surface of MoO_3.

First, we examined the cytotoxicity profiles of MoO_3 against keratinocyte HaCaT cells, breast cancer cell line MCF-7, and invasive MCF-7 (iMCF-7) using the MTT assay. There is no toxicity that was observed in HaCaT cells after exposure to MoO_3 (shown in SI Figure S4). The iMCF-7 cells were sorted from the normal breast cancer MCF-7 population using the stemness marker $CD44^{high}/CD24^{low}$. A wound-healing assay revealed that this new cell line is very aggressive, a property associated with stemness (shown in SI Figures S1−S3). A dose-dependent study compared these two cell types, and the cytotoxicity profiles are shown in Figure 4. Interestingly, the MoO_3 nanoplates inhibited the iMCF-7 cells more than the parental MCF7 cells. The IC_{50} of MoO_3 nanoplates toward iMCF-7 was 275 μg/mL. Therefore, MoO_3 nanoplates might be an alternative for the treatment of breast cancer stem cells.

To better understand the mechanism of the MoO_3-induced death of iMCF-7 cells, we examined whether the observed cell death was due to apoptosis using Hoechst 33342 staining. When apoptosis is induced, cells form apoptotic bodies that are distinguished by cell shrinkage and condensed, fragmented chromatin.[39] Figure 5 shows the Hoechst 33342 staining results using fluorescence microscopy. Clearly, the control cells did not show any apoptotic bodies, whereas the cells exposed to MoO_3 nanoplates showed the progressive accumulation (with different

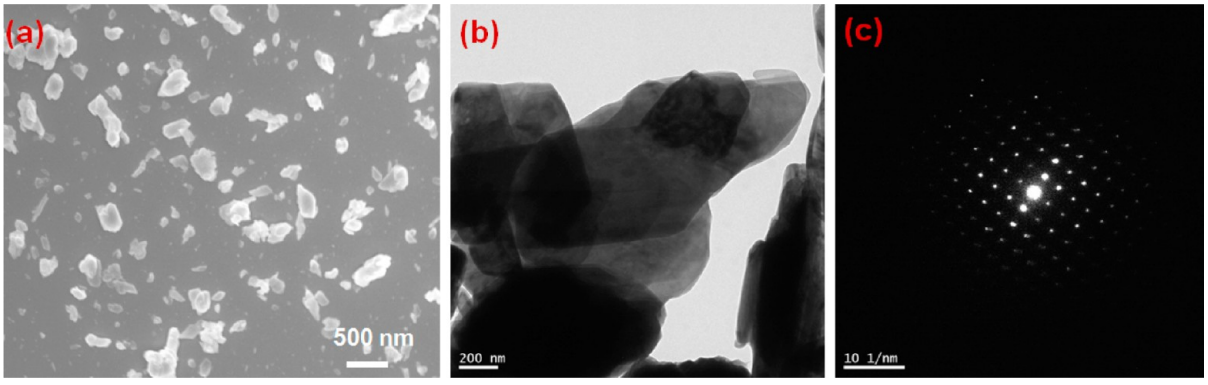

Figure 2. (a) Field emission-scanning electron microscope image, (b) high resolution transmission electron microscope image, and (c) selected area electron diffraction pattern of MoO_3 nanoplates.

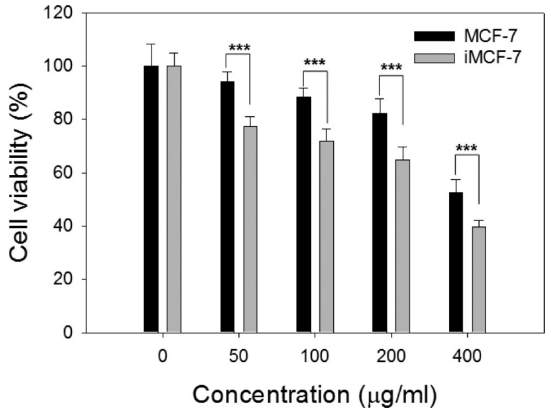

Figure 4. Cytotoxicity of MoO_3 nanoplates toward MCF-7 and iMCF-7 cells. Cells were performed MTT assay for 48 h with the indicated concentrations of MoO_3. Data are shown as means ± standard deviation (S.D.) Asterisks indicate significant difference in comparing MCF-7 and iMCF-7 ($p < 0.001$).

concentrations) of condensed, fragmented chromatin and apoptotic bodies (arrows) with the same morphology as the positive controls (quercetin treatment). This study confirms that the death of iMCF-7 cells is due to apoptosis.

The mechanism of cell death due to apoptosis involves DNA condensation and a reduction in the mitochondrial membrane potential and exposure of phosphatidylserine (PS) on the cell surface.[40,41] Apoptosis can occur via 1) extrinsic and 2) intrinsic pathways. The extrinsic pathway forms a death-inducing signaling complex (DISC) and involves caspase 8 and the death receptor. The intrinsic pathway takes place in mitochondria and involves cytochrome *c* and caspase 9. Hence, we used annexin V/PI and JC-1 fluorescence activated-cell sorting analysis (FACS) to detect the mitochondrial membrane potential (MMP) and PS. Annexin V staining has a high affinity for PS and can bind to intact cells with PS exposed at the outer membranes.[41] PI is a marker for dead or damaged cells because it can permeabilize into disrupted membranes.[42] The annexin V/PI result (Figure 6) showed increased annexin-V-positive cells following MoO_3 treatment for 48 h. This study revealed that MoO_3 induced early and late apoptosis in cancerous cells.

Mitochondria regulate apoptosis via the mitochondrial outer membrane potential (MOMP) and mitochondrial permeability transition (MPT). Opening the pores regulating the MOMP and MPT causes a loss of membrane potential ($\Delta\psi_m$). Cytochrome *c* and other apoptotic factors, such as apoptosis-inducing factor (AIF), endonuclease G, and caspase-activated DNase (CAD), are released to activate caspases, leading to DNA fragmentation.[43,44] Figure 7 shows the effect of MoO_3 NPs on the mitochondrial membrane potential in iMCF-7 cells. The nontoxic fluorescent probe JC-1 is concentrated in mitochondria as red fluorescent aggregates (FL2) when the membrane potential is high and is converted into green monomers (FL1) when $\Delta\psi_m$ is lost. Therefore, the loss of $\Delta\psi_m$ will lead to a decrease in FL2 or an increase in FL1.[45] As shown

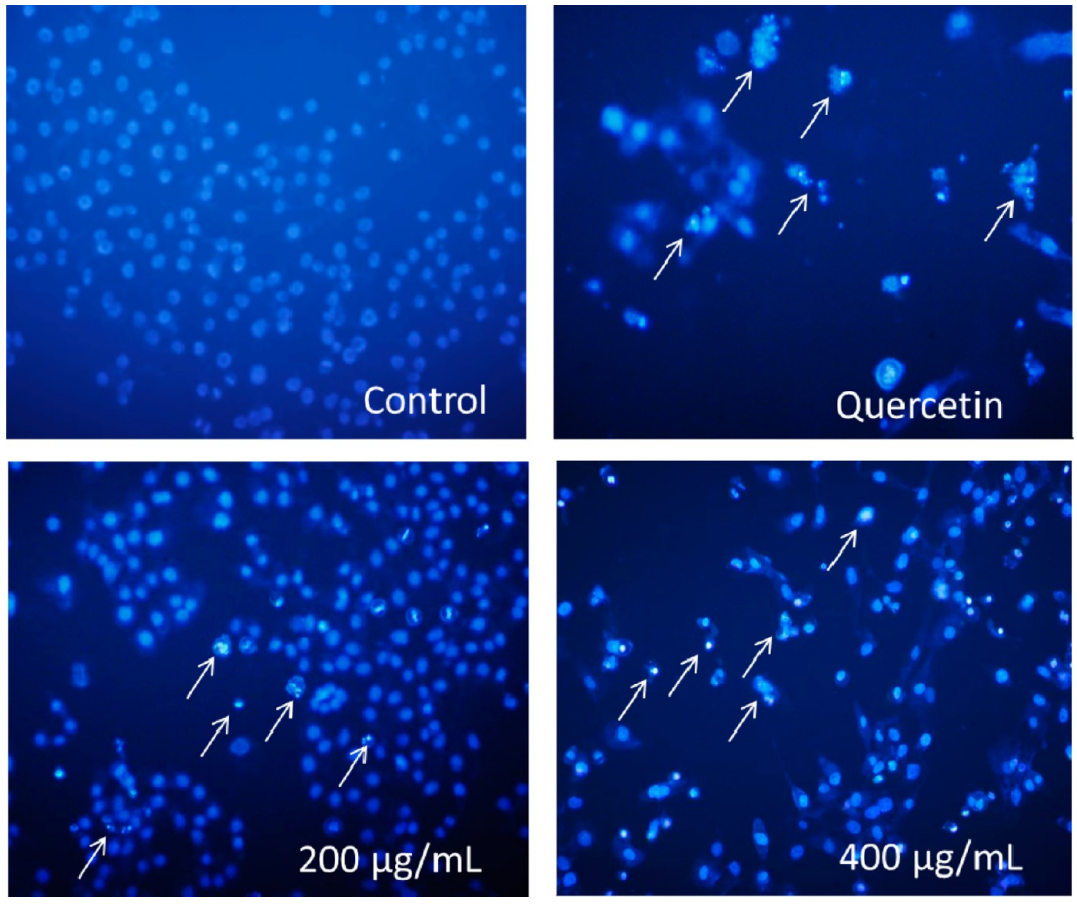

Figure 5. MoO_3 nanoplate-induced apoptosis in iMCF-7 cells. Treated cells were stained with Hoechst 33342 and observed under a fluorescence microscope. Arrows indicate cells with condensed and fragmented chromatins suggesting the apoptotic bodies.

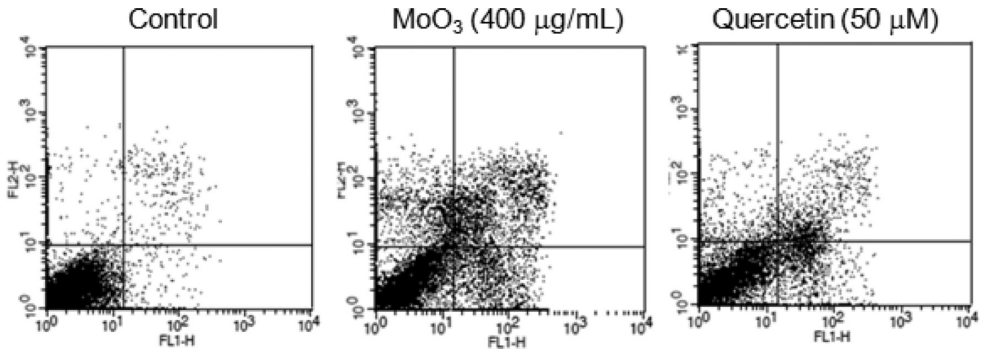

Figure 6. MoO_3 nanoplates induced Annexin V positive cells. iMCF-7 were treated for 48 h with MoO_3 at 400 μg/mL and quercetin at 50 μM. Cells were then harvested, stained with Annexin V/PI, and analyzed by flow cytometric analysis.

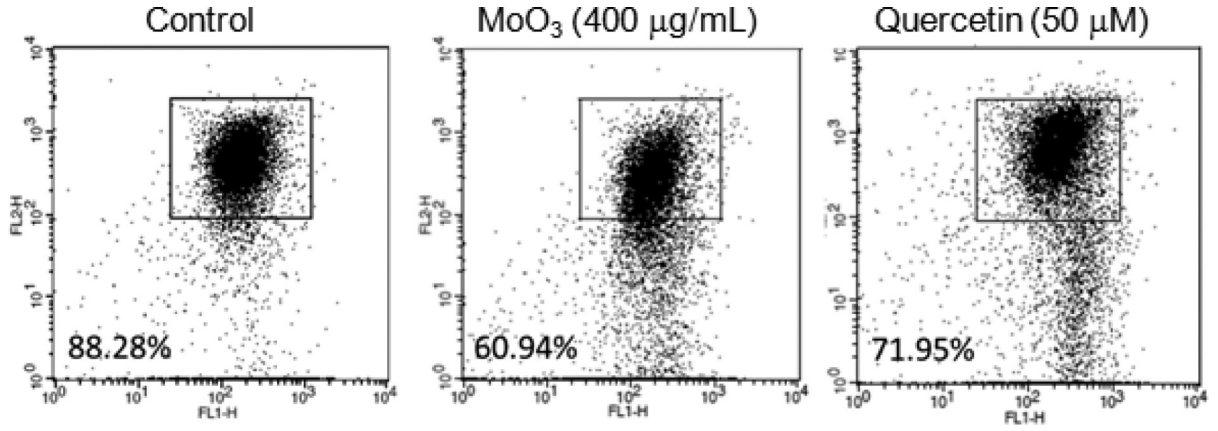

Figure 7. Effect of MoO_3 nanoplates on mitochondrial membrane potential ($\Delta\psi_m$) in iMCF-7 cells. Cells were treated with 400 μg/mL of MoO_3 nanoplates and quercetin at 50 μM for 48 h. Treated cells were harvested, then stained with JC-1, and analyzed by flow cytometric analysis.

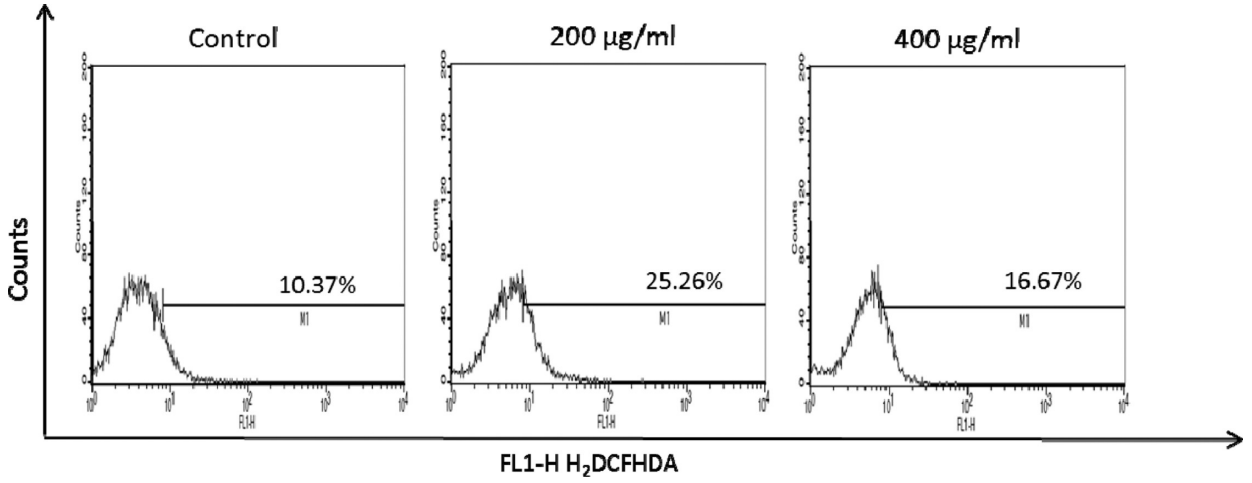

Figure 8. MoO_3 nanoplates increased the ROS production in iMCF-7 cells. Cells were treated with MoO_3 nanoplates at 200 and 400 μg/mL for 48 h. After 48 h, cells were incubated with H_2DCFHDA and then analyzed by flow cytometric analysis.

in Figure 7, MoO_3 NPs increased the number of mitochondria with disrupted membrane potentials in iMCF-7 cells at higher concentrations. This might trigger the release of pro-apoptotic proteins to activate caspases, further inducing apoptosis.

Oxidative stress is one of the most important mechanisms governing cell death due to nanomaterial-mediated toxicity.[46,47] The overproduction of ROS can lead to oxidative stress in cellular systems via a variety of stimuli that surpass the capacity of the intracellular antioxidant defense system, resulting in damage to cellular components.[5,48] In this study, we also investigated the ROS levels in cells treated with MoO_3 nanoplates using FACS analysis. First, iMCF-7 cells treated with appropriate concentrations of MoO_3 nanoplates loaded with H2DCFDA and their ROS levels were analyzed by flow cytometry. H2DCFDA (the reduced form of fluorescein) can be converted into its fluorescent form via the cleavage of acetate groups by intracellular esterases or oxidation. Figure 8 shows that the ROS levels were higher in the cells treated with MoO_3 nanoplates than the control cells. This demonstrates that the

dx.doi.org/10.1021/am405586d | ACS Appl. Mater. Interfaces 2014, 6, 2980−2986

mechanism of iMCF-7 cell death possibly involves elevated ROS levels.

To investigate the role of proteins in MoO_3-induced cell death, we performed Western blotting of apoptosis-related proteins exposed to MoO_3 nanoplates (Figure 9). The levels of

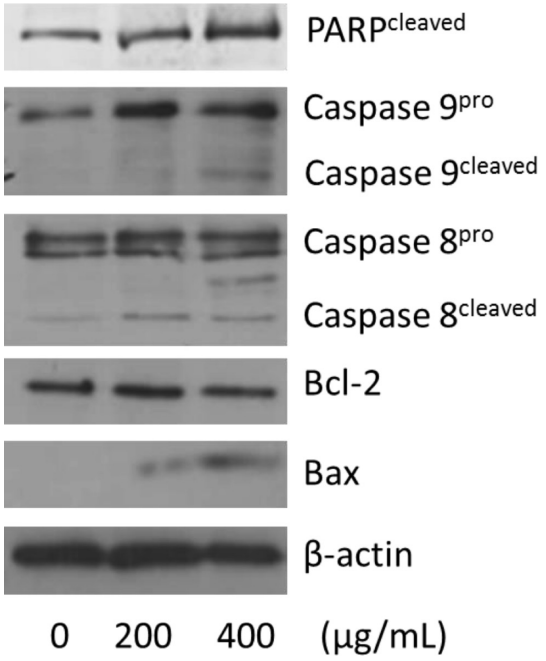

Figure 9. MoO_3 treatment induced intrinsic and extrinsic apoptosis in iMCF-7 cells. Cells were treated with MoO_3 nanoplates at 200 and 400 μg/mL for 48 h. Western blot analysis were performed with antibodies specific for cleaved PARP, caspase 9, caspase 8, Bcl-2, Bax, and β-actin.

the cleaved form of caspase 9, which is activated by the intrinsic pathway, increased. The level of Bax protein was enhanced, whereas that of Bcl-2 remained constant. This is consistent with the result in Figure 9. Bax and Bcl-2 are Bcl-2 family proteins that promote the opening of MOMP.[43] Bcl-2 is an antiapoptotic protein, whereas Bax is pro-apoptotic. The increasing Bax/Bcl-2 ratio indicated that mitochondria are permeabilized to release pro-apoptotic proteins. Interestingly, caspase 8, a well-known marker for the extrinsic pathway, and PARP-1, a marker for DNA damage, were also increased.[49] These results revealed that the cell death mechanism is activated via both the intrinsic and extrinsic apoptotic pathways. The mechanism of cellular toxicity of nanomaterials in biological systems is still debated due to the influence of factors such as size, shape, surface charge, and other physicochemical properties on toxicity.[6] Earlier studies demonstrated the oxidative stress mechanism of cell death due to ZnO, TiO_2, and CuO NP exposure.[16−18] The cytotoxicity of CeO_2 NPs is related to their regenerative antioxidant property.[50] Light-driven photocatalysis induced cell death in cells exposed to TiO_2.[16] Our previous study suggested the overproduction of ROS in AGS cells due to MgO NP exposure, which resulted in apoptotic death.[19] These studies suggest that several factors influence cancer cell death. In this study, the MoO_3 nanoplates showed significant toxicity toward MCF-7 and iMCF-7 cells. Figures 6 and 7 strongly suggest that the mechanism of iMCF-7 cell death upon exposure to MoO_3 nanoplates involved apoptosis via the loss of the mitochondrial membrane potential. The Western blotting results (shown in Figure 9) support this conclusion. Flow cytometry studies of the effect of ROS upregulation showed that the ROS levels were increased in iMCF-7 cells upon exposure to MoO_3 nanoplates (Figure 8). Overall, this study suggests that the toxicity of MoO_3 nanoplates toward iMCF-7 cells is a potential breakthrough in cancer therapy.

4. CONCLUSION

In conclusion, we demonstrated that MoO_3 nanoplates are cytotoxic toward iMCF-7 cells. The morphological studies and flow cytometry measurements together with the Western blotting suggested that the mechanism of cell death involves the apoptotic pathway via elevated ROS levels. This study revealed the potential utility of MoO_3 nanoplates for treating invasive breast cancer.

■ ASSOCIATED CONTENT

Supporting Information

Additional text and Figures S1−S4. This material is available free of charge via the Internet at http://pubs.acs.org.

■ AUTHOR INFORMATION

Corresponding Authors

*E-mail: kimsangj@jejunu.ac.kr (S.J.K.).
*E-mail: phd.kim.somi@gmail.com (S.K.C.).

Author Contributions

‡These authors contributed equally.

Notes

The authors declare no competing financial interest.

■ ACKNOWLEDGMENTS

This research was supported by Basic Science Research Program through National Research Foundation of Korea (NRF) funded by Ministry of Science, ICT & Future Planning (2013R1A1A2064471), and by Ministry of Education (2013R1A1A2A10012017).

■ REFERENCES

(1) Tarver, T. *J. Consum. Health Internet* **2012**, *16*, 366−367.
(2) Brabletz, T.; Jung, A.; Spaderna, S.; Hlubek, F.; Kirchner, T. *Nature* **2005**, *5*, 744−749.
(3) Burke, A. R.; Singh, R. N.; Carroll, D. L.; Wood, J. C.; D'Agostino, R. B., Jr.; Ajayan, P. M.; Torti, F. M.; Torti, S. V. *Biomaterials* **2012**, *33*, 2961−2970.
(4) Sanpui, P.; Chattopadhyay, A.; Ghosh, S. S. *ACS Appl. Mater. Interfaces* **2011**, *3*, 218−228.
(5) Premanathan, M.; Karthikeyan, K.; Jeyasubramanian, K.; Manivannan, G. *Nanomedicine: NBM* **2011**, *7*, 184−192.
(6) Raghupathi, K. R.; Koodali, R. T.; Manna, A. C. *Langmuir* **2011**, *5*, 4020−4028.
(7) Karthikeyan, K.; Babu, A.; Kim, S.-J.; Murugesan, R.; Jeyasubramanian, K. *Cancer Nanotechnol.* **2011**, *2*, 95−103.
(8) Hu, Z.; Li, J.; Li, C.; Zhao, S.; Li, N.; Wang, Y.; Wei, F.; Chen, L.; Huang, Y. *J. Mater. Chem. B* **2013**, *1*, 5003−5013.
(9) Shen, J. M.; Yin, T.; Tian, X.-Z.; Gao, F.-Y.; Xu, S. *ACS Appl. Mater. Interfaces* **2013**, *5*, 7014−7024.
(10) Di, D. R.; He, Z. Z.; Sun, Z. Q.; Liu, J. *Nanomedicine: NBM* **2012**, *8*, 1233−1241.
(11) Harada, A.; Ono, M.; Yuba, E.; Kono, K. *Biomater. Sci.* **2013**, *1*, 65−73.
(12) Yang, K.; Wan, J.; Zhang, S.; Tian, B.; Zhang, Y.; Liu, Z. *Biomaterials* **2012**, *33*, 2206−2214.

(13) Meng, Y.; Zou, C.; Madiyalakan, R.; Woo, T.; Huang, M.; Yang, X.; Swanson, E.; Chen, J.; Xing, J. Z. *Nanomedicine* **2010**, *5*, 1559−1569.
(14) Niu, A.; Han, Y.; Wu, J.; Yu, N.; Xu, Q. *J. Phys. Chem. C* **2010**, *114*, 12728−12735.
(15) Zhou, W.; Liu, X.; Ji, J. *J. Mater. Chem.* **2012**, *22*, 13969−13976.
(16) Thevenot, P.; Cho, J.; Wavhal, D.; Timmons, R. B.; Tang, L. *Nanomedicine: NBM* **2008**, *4*, 226−236.
(17) Lin, W.; Huang, Y. W.; Zhou, X. D.; Ma, Y. *Int. J. Toxicol.* **2006**, *25*, 451−457.
(18) Wang, Y.; Zi, X. Y.; Su, J.; Zhang, H. X.; Zhang, X. R.; Zhu, H. Y.; Li, J. X.; Yin, M.; Yang, F.; Hu, Y. P. *Int. J. Nanomed.* **2012**, *7*, 2641−2652.
(19) Krishnamoorthy, K.; Moon, J. Y.; Hyun, H. B.; Cho, S. K.; Kim, S.-J. *J. Mater. Chem.* **2012**, *22*, 24610−24617.
(20) Cheng, L.; Shao, M.; Wang, X.; Hu, H. *Chem.—Eur. J.* **2009**, *15*, 2310−2316.
(21) Murugan, A. V.; Viswanath, A. K.; Gopinath, C. S.; Vijayamohanan, K. *J. Appl. Phys.* **2006**, *100*, 074319.
(22) Yoshida, M.; Hattoria, H.; Otaa, S.; Yoshihara, K.; Kodama, N.; Yoshitake, Y.; Nishimuta, M. *J. Trace Elem. Med. Biol.* **2006**, *20*, 245−252.
(23) Keshavarzi, B.; Moore, F.; Najmeddin, A.; Rahmani, F. *Sci. Total Environ.* **2012**, *433*, 89−97.
(24) Levina, A.; McLeod, A. I.; Seuring, J.; Lay, P. A. *J. Inorg. Biochem.* **2007**, *101*, 1586−1593.
(25) Krishnamoorthy, K.; Veerapandian, M.; Yun, K.; Kim, S. J. *Colloids Surf., B* **2013**, *112*, 521−524.
(26) Hussain, S. M.; Hess, K. L.; Gearhart, J. M.; Geiss, K. T.; Schlager, J. J. *Toxicol. In Vitro* **2005**, *19*, 975−983.
(27) Stolle, L. B.; Hussain, S.; Schlager, J. J.; Hofmann, M. C. *Toxicol. Sci.* **2005**, *88*, 412−419.
(28) Ogata, A.; Yanagie, H.; Ishikawa, E.; Morishita, Y.; Mitsui, S.; Yamashita, A.; Hasumi, K.; Takamoto, S.; Yamase, T.; Eriguchi, M. *Br. J. Cancer* **2008**, *98*, 399−409.
(29) Mitsui, S.; Ogata, A.; Yanagie, H.; Kasano, H.; Hisa, T.; Yamase, T.; Eriguchi, M. *Biomed. Pharmacother.* **2006**, *60*, 353−358.
(30) Carmichael, J.; Degraff, W. G.; Gazdar, A. F.; Minna, J. D.; Mitchell, J. B. *Cancer Res.* **1987**, *47*, 936−942.
(31) Mai, T.-T.; Moon, J.-Y.; Song, Y.-W.; Viet, P.-Q.; Phuc, P.-V.; Lee, J.-M.; Yi, T.-H.; Cho, M.; Cho, S.-K. *Cancer Lett.* **2012**, *321*, 144−153.
(32) Parrilla, I.; Vazquez, J. M.; Cuello, C.; Gil, M. A.; Roca, J.; Berardino, D. D.; Martınez, E. A. *Reproduction* **2004**, *128*, 615−621.
(33) Moon, J.-Y.; Mosaddik, A.; Kim, H.; Cho, M.; Choi, H.-K.; Kim, Y. S.; Cho, S.-K. *Food Chem.* **2011**, *125*, 369−375.
(34) Tang, W.; Liu, L.; Tian, S.; Li, L.; Yue, Y.; Wu, Y.; Zhu, K. *Chem. Commun.* **2011**, *47*, 10058−10060.
(35) Chen, S.; Guo, Y.; Chen, S.; Yu, H.; Ge, Z.; Zhang, X.; Zhang, P.; Tang, J. *J. Mater. Chem.* **2012**, *22*, 9092−9099.
(36) Pacchioni, G. *ChemPhysChem* **2003**, *4*, 1041−1047.
(37) Song, J.; Ni, X.; Zhang, D.; Zheng, H. *Solid State Sci.* **2006**, *8*, 1164−1167.
(38) Navas, I.; Vinodkumar, R.; Mahadevan Pillai, V. P. *Appl. Phys. A: Mater. Sci. Process.* **2011**, *103*, 373−380.
(39) Salvioli, S.; Ardizzoni, A.; Franceschi, C.; Cossarizza, A. *FEBS Lett.* **1997**, *411*, 77−82.
(40) Sun, X. M.; MacFarlane, M.; Zhuang, J.; Wolf, B. B.; Green, D. R.; Cohen, G. M. *J. Biol. Chem.* **1999**, *274*, 5053−5060.
(41) Engeland, M.; Nieland, L. J.; Ramaekers, F. C.; Schutte, B.; Reutelingsperger, C. P. *Cytometry* **1998**, *31*, 1−9.
(42) Lecoeur, H. *Exp. Cell Res.* **2002**, *277*, 1−14.
(43) Danial, N. N.; Korsmeyer, S. J. *Cell* **2004**, *116*, 205−219.
(44) Javadov, S.; Karmazyn, M. *Cell Physiol. Biochem.* **2007**, *20*, 1−22.
(45) Chen, M.; Zsengeller, Z.; Xiao, C. Y.; Szabo, C. *Cardiovasc. Res.* **2004**, *63*, 682−688.
(46) Guo, D.; Bi, H.; Liu, B.; Wu, Q.; Wang, D.; Cui, Y. *Toxicol. In Vitro* **2013**, *27*, 731−738.
(47) Krishnamoorthy, K.; Veerapandian, M.; Zhang, L.-H.; Yun, K.; Kim, S.-J. *J. Phys. Chem. C* **2012**, *116*, 17280−17287.
(48) Xia, T.; Kovochich, M.; Brant, J.; Hotze, M.; Sempf, J.; Oberley, T.; Sioutas, C.; Yeh, J. I.; Wiesner, M. R.; Nel, A. E. *Nano Lett.* **2006**, *6*, 1794−1807.
(49) Gobeil, S.; Boucher, C. C.; Nadeau, D.; Poirier, G. G. *Nature* **2001**, *8*, 588−591.
(50) Wason, M. S.; Colon, J.; Das, S.; Seal, S.; Turkson, J.; Zhao, J.; Baker, C. H. *Nanomedicine: NBM* **2013**, *9*, 558−569.